Zhao, P., et al., 2021, Early Neoproterozoic (870–820 Ma) amalgamation of the Tarim craton (northwestern China) and the final assembly of Rodinia: Geology, v. 49, https://doi.org/10.1130/G48837.1

Supplementary Material for:

Early Neoproterozoic (870-820 Ma) amalgamation of the Tarim Craton and the final assembly of Rodinia

Pan Zhao, Jinyou He, Chenglong Deng, Yan Chen, and Ross Mitchell

This file contains:

Supplementary text

Supplementary figures (Fig. S1, S2)

Supplementary tables (Table S1, S2, S3)

Supplementary references

SUPPLEMENTARY TEXT

Paleomagnetic sampling and laboratory procedure

The paleomagnetic samples were collected from the newly identified Qigelekekuotan volcanic sequence (QV; Fig. S2). In total, 21 sites (194 cores) were drilled using a portable gasoline drilling machine. Cores were orientated in the field by both magnetic and solar compasses.

In the laboratory, core samples (2.5 cm in diameter) were cut into standard cylinder specimens with 2.2 cm in height. Systematic rock magnetic investigations were performed to determine the magnetic carrier(s). High-temperature thermomagnetic experiments (κ-T) were performed using a MFK-1 Kappa-bridge coupled with a CS3 furnace. Acquisition and back-field demagnetization of isothermal remanent magnetization (IRM) and magnetic hysteresis loops were measured using a MicroMag 3900 Alternating Gradient Magnetometer with an applied filed in the range of ± 1.5 T. All these magnetic mineralogy investigations were conducted in the Paleomagnetism and Geochronology Laboratory (PGL) of the Institute of Geology and Geophysics, Chinese Academy of Sciences.

All standard specimens were subjected to stepwise demagnetization. Only thermal demagnetization technique was applied to remove the magnetic remanence progressively by 13-16 steps up to 685˚C, with temperature intervals of 20˚C to 100˚C. A thermal demagnetizer (model TD-48SC of the ASC Scientific Company) was used for demagnetization, which is followed by magnetic remanence measurement with a 2G Enterprises three-axis SQUID Magnetometer (Model 755) installed in a magnetically shielded room with residual field of less than 200 nT in the PGL.

Magnetic directions were analyzed by principal component analysis (Kirschvink, 1980).

Mean remanence directions were computed by Fisher statistics by paleomagnetic software packages of Remasoft (designed by AGICO) and PaleoMac (Cogné, 2003).

Rock magnetism

Rock magnetic experiments Thermomagnetic (κ-T) curves show irreversible heating and cooling behaviors (Figs. S2A-C). The heating curves show a significant decrease of the magnetic susceptibility values at ~580°C, and then a gradual decay until 700°C (Figs. S2A-C), indicating the existence of both magnetite and hematite as magnetic remanence carriers. The hysteresis loops of studied samples (Figs. S2D-F) show wasp-waisted shape with coercivity (Hc) values of 48-90 mT and Mr/Ms ratios at ~0.4, suggesting that both soft (magnetite) and hard (hematite) magnetic minerals exist as magnetic carriers. IRM acquisition curves show a rapid increase of magnetization from 0-200 mT, followed by a gradual increase of magnetization without saturation at 1.5 T (Figs. S2G-I), indicating the coexistence of magnetite and hematite. Unmixing of magnetic mineral components also reveals both soft and hard mineral components (Figs. S2J-L). From rock magmatic experiments, magnetite and hematite can be considered as the main magnetic remanence carriers in the studied volcanic samples.

Reference:

Cogné, J.P., 2003, A Macintosh™ application for treating paleomagnetic data and making plate reconstructions: Geochemistry, Geophysics, Geosystems, v. 4, p. 1007, doi:10.1029/2001GC000227.

Kirschvink, J.L., 1980, The least-squares line and plane and the analysis of paleomagnetic data: Geophys. J. R. Astron. Soc., v. 62, p. 699–718, doi:10.1111/j.1365-246X.1980.tb02601.X.

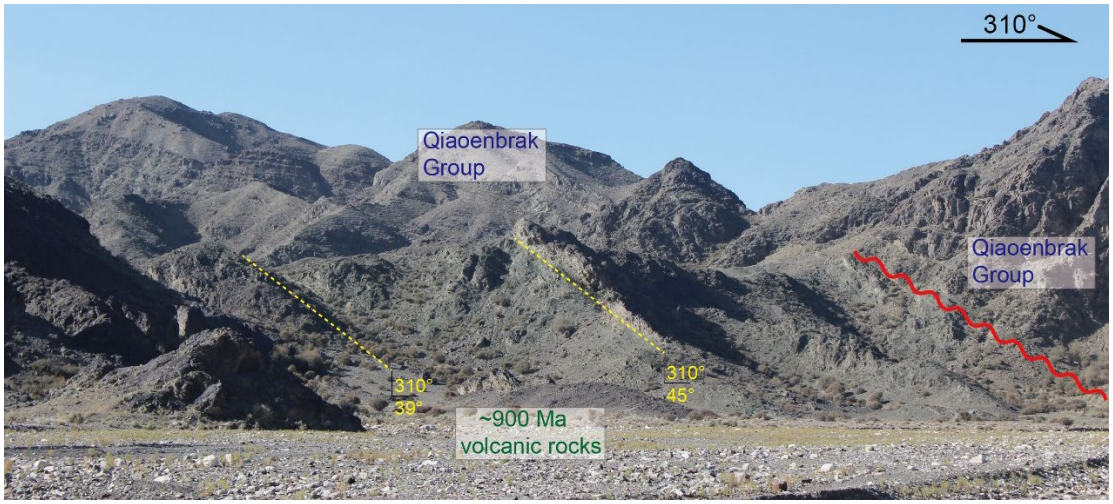

Fig. S1: Photo of field outcrop of the ~900 Ma Qigelekekuotan volcanic sequence showing dip and unconformable relationship with the Qiaoenbrak Group.

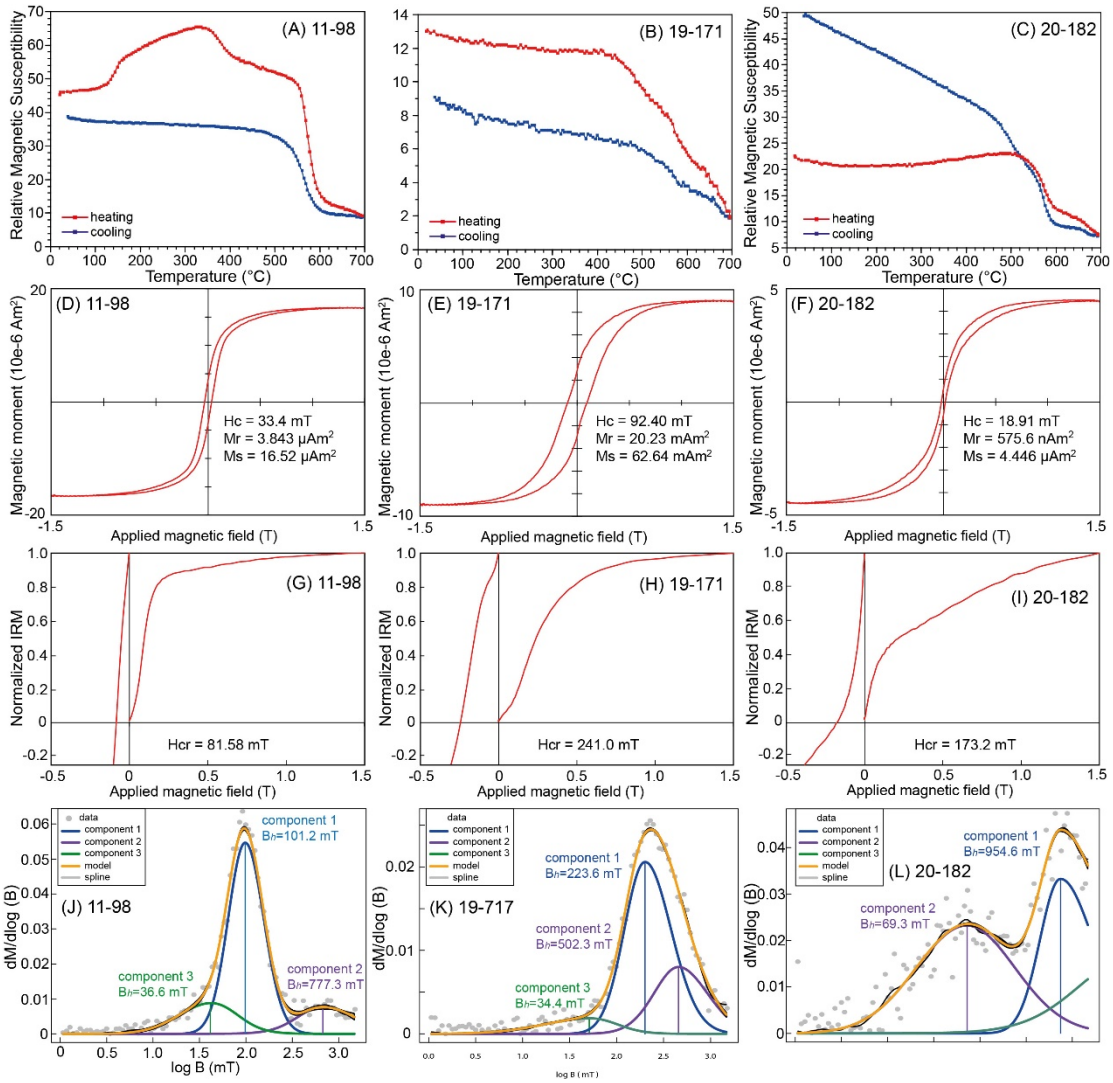

Fig. S2: Rock magnetic experiments. Thermomagnetic curves of magnetic susceptibility (A-C), magnetic hysteresis loops (D-F), isothermal magnetization acquisition and back-field demagnetization of saturation IRM (SIRM) acquisition curves (G-I), and unmixing of magnetic mineral components modeled with MAX UnMix (J-L) of selected samples.

SUPPLEMENTARY TABLES

Table S1: Paleomagnetic sampling and measurement results of the ~900 Ma volcanic rocks from the Aksu region in northwestern Tarim craton

Table S2: Paleomagnetic poles for the Tarim craton from the Neoproterozoic to present.

Table S3: Compilation of 1000-850 Ma palaeomagnetic poles from main cratons of Rodinia. Abbreviations: Slat (Plat), latitude of sampling site (pole); Slong (Plong), longitude of sampling site (pole); A_{95}, 95% confidence limit; FT, fold test; CT, conglomerate test; BT, backed test; N+R, existence of both normal and reversed polarities.

Table S1. Paleomagnetic sampling and measurement results of the ~900 Ma volcanic rocks from the Aksu region in northwestern Tarim Craton

Site	coordinate	rock type	dip dir./angle	n'/n	N/R	Dg	Ig	Ds	Is	k/K	α_{95}/A_{95}	*s/S*	Plat. (°N)	Plong. (°E)
01-03	40°56'38"N, 79°30'12"E	feldspar-phenocryst-bearing andesite	315/40	6/24	5/1	182.6	34.9	219.7	52.6	41.2	10.6	13.6	-7.4	46.9
04	40°56'39"N, 79°30'13"E	feldspar-phenocryst-bearing andesite	315/40	7/8	7/0	197.7	45.1	243.3	48.7	70.9	7.2	25.5	1.6	28.5
05	40°56'39"N, 79°30'13"E	feldspar-phenocryst-bearing andesite	315/40	0/6	0/0	-	-	-	-	-	-			
06	40°56'39"N, 79°30'14"E	feldspar-phenocryst-bearing andesite	315/40	6/13	6/0	131.0	22.1	187.6	49.9	49.2	9.9	16.9	-18.1	72.6
07*	40°56'40"N, 79°30'13"E	feldspar-phenocryst-bearing andesite	315/40	7/7	7/0	253.7	52.9	279.3	25.1	24.1	12.5	60.7	15.6	353.6
08	40°56'43"N, 79°30'10"E	green andesite	310/45	12/13	12/0	159.9	36.8	210.5	66.1	16.9	10.9	3.1	3.3	59.8
09	40°56'44"N, 79°30'10"E	green andesite	310/45	7/7	7/0	135.8	24.5	144.9	68.9	57.4	8.0	23.6	8.1	100.3
10	40°56'44"N, 79°30'10"E	green andesite	310/45	7/7	7/0	133.2	26.3	138.8	71.1	26.6	11.9	24.9	12.6	101.9
11	40°56'43"N, 79°30'09"E	green andesite	310/45	9/9	9/0	149.8	33.5	189.9	71.0	56.3	6.9	9.1	6.7	73.9
12	40°56'43"N, 79°30'09"E	green andesite	310/45	8/8	8/0	149.2	21.1	169.7	61.3	34.2	9.6	16.3	-6.2	87.1
13	40°56'44"N, 79°30'14"E	green andesite	310/39	6/9	6/0	143.0	45.0	191.1	79.5	61.6	8.6	16.0	20.9	75.4
14	40°56'09"N, 79°30'43"E	purple andesite	265/26	9/9	9/0	181.5	64.7	221.0	52.4	35.9	8.7	14.2	-7.0	45.8
15	40°56'09"N, 79°30'43"E	purple andesite	265/26	8/8	8/0	168.3	69.5	222.1	59.3	235.0	3.6	9.3	-0.4	48.6
16*	40°56'09"N, 79°30'43"E	purple andesite	265/26	7/10	7/0	322.4	68.8	292.6	48.8	25.5	12.2	46.5	35.2	0.5
17*	40°56'09"N, 79°30'43"E	purple andesite	265/26	10/10	10/0	312.7	67.2	289.1	45.6	19.0	11.4	47.6	31.2	359.8
18	40°56'09"N, 79°30'44"E	green andesite	265/26	4/5	0/4	13.3	-68.5	50.8	-51.8	56.8	12.3	18.0	-3.0	38.6
19	40°56'10"N, 79°30'42"E	purple andesite	265/26	3/9	3/0	171.3	74.7	232.1	61.0	87.2	13.3	12.7	5.4	43.4
20	40°56'18"N, 79°30'32"E	green tuff	265/26	10/10	10/0	155.0	62.5	204.6	60.0	50.7	6.9	4.0	-5.2	61.1
21	40°56'18"N, 79°30'32"E	green tuff	265/26	11/11	11/0	141.4	54.9	183.6	61.0	131.7	4.0	10.4	-7.0	76.8
	Mean (15 sites)					***155.2***	***47.5***			***11.6***	***11.7***			
								205.2	***64.0***	***24.4***	***7.9***			
VPGs mean										***11.5***	***11.8***	***23.3***	**0.3**	**63.8**

Abbreviations: n'/n: numbers of accepted/measured samples; N/R: normal/reverse polarity; Dg, Ig, Ds, Is: declination (D) and inclination (I) in geographic (g) and tilt-corrected (s) coordinates; k/K: precision parameter for site-mean direction and formation mean virtual geomagnetic pole (VGP); α_{95}/A_{95}: radius of the 95% confidence circle for site-mean direction and formation mean VGP. Plong/Plat, longitude/latitude of VGP after tilt correction. *s/S*, angular deviations of site-mean directions and VGPs. *Sites were discarded for further discussion due to >45° angular deviations from mean direction. VGPs are calculated at reference site 40.9°N and 79.5°E. Paleolatitude = 47.0˚ ± 11.8˚N is calculated with VGPs mean.

McElhinny's (1964) fold test: ks/kg = 2.10 > 1.88; indicate positive fold test at 95% confidence level.

McFadden's (1990) fold test: $\xi_2 = 9.819$ before, and $\xi_2 = 0.3884$ after tilt correction, critical value $\xi = 4.510$ at 95% and $\xi = 6.305$ at 99% confidence level; indicate positive fold test at 99% confidence level.

Enkin's (2003) DC fold test give positive feedback with DC Slope: 97.03 % ± 21.48% untilting.

Watson and Enkin's (1993) fold test give optimum degree of untilting at 96.0% ± 12.2%, indicating positive fold test.

The angular deviation of the 15 corresponding virtual geomagnetic poles (VGPs) (S=23.3° at 47°) is similar with S_λ = 17.1° (95% confidence limits of 14.3°-20.4°) at 43.1°N and S_λ = 20.7° (95% confidence limits of 18.2°-23.4°) at 53.1°N (Johnson et al., 2008). The A_{95} value of the mean VGPs fall in the range of A_{95} envelope defined by Deenen et al. (2011) (A_{95} min = 4.1° < A_{95} = 11.8° < A_{95} max = 14.9°). These results indicate that paleosecular variation has been averaged out.

Table S2. Paleomagnetic poles for the Tarim Craton from the Neoproterozoic to present

Age	S(N)	SLAT	SLON	PLAT	PLON	Dp/A_{95}	Dm	Reference	Comment
Neoproterozoic									
*NP1, 909-903	15	40.9	79.5	-0.5	62.2	11.2		This study	FT, N+R
*NP1, 900-870	11	37.0	77.3	-23.5	37.0	11.3		Wen et al., 2018	CT
*NP2, 785-759	9	41.1	80.1	19.0	128.0	6.0	7.0	Chen et al., 2004	N+R
*NP2, 750-725	6	41.6	86.5	-17.7	14.2	3.0	6.0	Huang et al., 2005	
*NP2, 730	14	40.9	79.5	-6.3	17.5	9.1		Wen et al., 2013	CT, N+R
*NP2, 635	6	41.5	87.8	27.6	140.4	8.8	11.1	Zhao et al., 2014	FT
*NP2, 625	24	41.0	80.0	19.1	149.7	9.3		Zhan et al., 2007	FT, N+R
*NP2, 625	36	41.0	79.3	-21.1	87.4	7.0		Wen et al., 2017	FT, N+R
*NP2, 615	8	41.5	87.8	-4.9	146.7	3.0	5.2	Zhao et al., 2014	
Early Ordovician									
* 480	5	41.3	83.4	-20.4	180.6	8.5	15.0	Zhu et al., 1998	
Middle Ordovician									
* 460	11	40.6	78.9	-33.7	185.0	2.7	4.0	Huang et al., 2019	N+R
Silurian									
* 435	6	40.5	79.7	12.1	158.4	4.1	7.2	Zhu et al., 1998	
Middle Silurian									
* 430	10	40.5	78.7	19.1	172.9	5.5		Huang et al., 2019	FT, N+R
Early-middle Devonian									
* 400	3	40.5	79.6	13.5	160.8	4.9		Fang et al, 1996	
Late Devonian									
* 370	47	40.5	78.6	16.5	165.0	4.3		Li et al, 1990	FT, N+R
Late Carboniferous									
C_2	4	40.3	79.5	52.2	179.5	6.8	10.7	Bai et al., 1987	
C_2	3			48.7	175.7	3.0	4.8	Fang et al., 1998	
***Ave, 310**	**2/2**			**50.5**	**177.5**	**9.3**			
Early Permian									
P_1	5	40.6	79.5	56.1	179.4	2.5		Fang et al., 1998	FT
P_1	21	40.5	78.8	54.5	172.3	4.0		Sharps et al., 1989	
***Ave, 280**	**2/2**			**55.4**	**175.8**	**9.5**			
Late Permian									
P_2	7	44.0	88.1	75.8	195.0	13.6	18.5	Nie et al., 1991	FT, N+R
P_2	10	42.1	83.4	73.2	191.0	7.2	10.3	McFadden et al., 1988	N+R
P_3	21	40	79	65.6	181.2	3.9		Li et al., 1988,	N+R
P_3-T_1	16	42.1	83.3	71.8	187.6	5.5	7.8	McFadden et al., 1988	FT
***Ave, 255**	**4/4**			**71.2**	**186.7**	**4.0**			

Triassic									
T_1	5	41	74.9	52.8	175.5	6.3	10.1	Zhu et al., 1998	N+R
T_2	26	40.9	81.5	52.5	168.2	4.2	6.1	Zhu et al., 1998	N+R
T_3	8	41.7	80.5	52.1	166.8	5.6	8.1	Zhu et al., 1998	N+R
T	6	41.6	83.5	59	160	13		Li et al., 1990	FT, N+R
***Ave, 230**	**4/4**			**54.2**	**167.9**	**5.6**			
Middle Jurassic									
*170	10	36	79.2	53.9	186.4	4.4	7.6	Zhu et al., 1998	N+R
Late Jurassic									
*155	6	41.7	80.5	68.6	171.8	5.7	7.8	Fang et al., 1998	N+R
Early Cretaceous									
J_3-K_1	13	44.2	86.0	72.3	227.3	4.8	7.2	Chen et al., 1991	FT, N+R
J_3-K_1	6	41.8	82.0	65.0	209.0	9	9	Li et al., 1988	N+R
K_1	7	39.5	75	66.3	226.6	9	15.9	Chen et al., 1992	N+R
K_1	3	38.5	76.4	70.4	212.1	6.6	10.8	Chen et al., 1992	N+R
K_1	8	36.3	78.8	72.3	206.6	9.8	15.9	Zhu et al., 1998	FT, N+R
***Ave, 120**	**5/5**			**69.5**	**216.3**	**4.6**			
Late Cretaceous									
K_2	7	41.6	83.5	66.3	222.9	8.7	8.7	Li et al., 1988	FT
K_2	10	42	82.9	64	229	7.3	12.7	Zhu et al., 1998	N+R
K_2	11	39.5	75	70.8	222.6	5.4	8.9	Chen et al., 1992	FT
K_2	6	38.5	76.4	71	234	6.8	11.6	Chen et al., 1992	N+R
K_2-E	9	44.2	86.0	74.3	223.1	6.4	9.4	Chen et al., 1991	FT, N+R
***Ave, 80**	**5/5**			**69.3**	**226.4**	**4.2**			
Paleogene									
*50	4	41.6	83.5	73	245.4	6.0	9.7	Fang et al., 1998	
Quaternary									
*2	3	36.2	81.5	79.9	183.1	1.6	2.4	Meng et al., 1998	

Poles with * were plotted in figure S3.

Abbreviations: S/N, the number of sites/drilled cores; Slong/Slat, longitude and latitude of sampling site; Plat/Plong, latitude and longitude of paleomagnetic pole; Dp/Dm, oval of 95% confidence for the paleomagnetic pole; A_{95}, radius that mean direction lies within 95% confidence. FT, fold test; CT, conglomerate test; N+R, existence of both normal and reversed polarities.

References:

Bai, Y.H., Chen, G.L., Sun, Q.G., Sun, Y.H., Li, Y.A., Dong, Y.J., Sun, D.J., 1987. Late Pale-ozoic polar wander path for the Tarim platform and its tectonic significance.Tectonophysics 139, 145–153.

Chen, Y., Cogné, J.P., Courtillot, V., 1992. New paleomagnetic poles from the TarimBasin, Northwestern China. Earth Planet. Sci. Lett. 114, 17–38.

Chen, Y., Cogné, J.P., Courtillot, V., Avouac, J.Ph., Tapponnier, P., Buffetaut, E., Wang, G.,Bai, M., You, H., Li, M., Wei, C., 1991. Paleomagneitc study of Mesozoic continentalsediments along the northern

Tien Shan (China) and heterogeneous strain incentral Asia. J. Geophys. Res. 96, 4065–4082.

Chen, Y., Xu, B., Zhan, S., Li, Y.A., 2004. First mid-Neoproterozoic paleomagnetic results from the Tarim Basin (NW China) and their geodynamic implications. Precambrian Res.133, 271–281.

Fang, D.J., Jin, G.H., Jiang, L.P., Wang, P.Y., Wang, Z.L., 1996. Paleozoic paleomagneticresults and the tectonic significance of Tarim palte. Acta Geophys. Sin. 39 (4),522–532 (in Chinese with English abstract).

Fang, D.J., Wang, P.Y., Shen, Z.Y., Tan, X.D., 1998. Paleomagnetic results and Phanero-zoic apparent polar wandering path of Tarim block. Sci. China Ser. D 41 (Suppl.),105–112.

Huang, B.C., Xu, B., Zhang, C.X., Li, Y.A., Zhu, R.X., 2005. Paleomagnetism of the Baiy-isi volcanic rocks (ca. 740 Ma) of Tarim Northwest China: a continental fragment of Neoproterozoic Western Australia? Precambrian Res.142, 83–92.

Li, Y.P., McWilliams, M., Cox, A., Shrarps, R., Li, Y., Gao, Z., Zhang, Z., Zhai, Y., 1988. Late Permian Paleomagnetic pole from dikes of the Tarim craton, China. Geology16, 275–278.

Li, Y.P., McWilliams, M., Sharps, R., Li, Y.A., Gao, Z.J., 1990. A Devonian paleomagneticpole from red beds of the Tarim Block, China. J. Geophys. Res. 98, 185–198.

McFadden, P.L., Ma, X.H., McElhinny, M.W., Zhang, Z.K., 1988. Permo-Triassic mag-netostratigraphy in China: northern Tarim. Earth Planet. Sci. Lett. 87, 152–160.

Meng, Z.F., Deng, Y.S., Ding, Z.H., Zheng, Y.P., Li, Y.A., Sun, D.J., 1998. New paleo-magnetic results from Ceno-Mesozoic volcanic rocks along southern rim of theTarim Basin, China. Sci. China Ser. D 41 (Suppl.), 91–104.

Nie, S.Y., 1991. Paleoclimatic and paleomagnetic constraints on the Paleozoic recon-struction of south China, north China and Tarim. Tectonophysics 196, 279–308.

Sharps, R., McWilliams, M., Li, Y.P., Cox, A., Zhang, Z.K., Zhai, Y.J., Gao, Z.J., Li, Y.A.,Li, Q., 1989. Lower Permian paleomagnetism of the Tarim block, northwesternChina. Earth Planet. Sci. Lett. 92, 275–291.

Wen, B., Evans, D.A.D., and Li, Y.X., 2017, Neoproterozoic paleogeography of the Tarim Block: An extended or alternative “missing-link” model for Rodinia?: Earth and Planetary Science Letters, v. 458, p. 92–106, https:// doi.org/10.1016/j .epsl.2016 .10 .030.

Wen, B., Evans, D.A.D., Wang, C., Li, Y.X., and Jing, X., 2018, A positive test for the Greater Tarim Block at the heart of Rodinia: Mega-dextral suturing of supercontinent assembly: Geology, v. 46(8), p. 687-690, https://doi.org/10.1130/G40254.1

Wen, B., Li, Y.X., Zhu, W.B., 2013. Paleomagnetism of the Neoproterozoic diamictites of the Qiaoenbrak formation in the Aksu area, NW China: constraintson the paleogeographic position of the Tarim Block. Precambrian Res.226, 75–90.

Zhan, S., Chen, Y., Xu, B., Wang, B., Faure, M., 2007. Late Neoproterozoic paleomag-netic results from the Sugetbrak Formation of the Aksu area, Tarim basin (NW China) and their implications to paleogeographic reconstructions and the snow-ball Earth hypothesis. Precambrian Res.154, 143–158.

Zhao, P., Chen, Y., Zhan, S., Xu, B., Faure, M., 2014. The apparent polar wander path of the Tarim block (NW China) since the Neoproterozoic and its implications for a long-term Tarim–Australia connection. Precambrian Res.242, 39–57.

Zhu, R.X., Yang, Z.Y., Wu, H.N., Ma, X.H., Huang, B.C., Meng, Z.F., Fang, D.J., 1998.Paleomagnetic apparent polar wander paths and movement for China maincontinental blocks during Phanerozoic. Sci. China Ser. D 28 (Suppl.), 1–16.

Table S3. Compilation of 1000-800 Ma palaeomagnetic poles from main cratons of Rodinia. Abbreviations: Slat (Plat), latitude of sampling site (pole); Slong (Plong), longitude of sampling site (pole); A_{95}, 95% confidence limit; FT, fold test; CT, conglomerate test; BT, backed test; N+R, existence of both normal and reversed polarities.

Pole ID	Age	location	Rock unit	Plat (°N)	Plong (°E)	A_{95}(°) (dp/dm)	paleolatitude (°N)	Test	References
Tarim									
QV	909-903	Aksu	Qigelekekuotan volcanics	-0.5	62.3	11.8	47.0 ± 11.8	FT, N+R	This study
SGV	890-870	Yecheng	Sailajiazitage Group volcanics	-23.5	37.0	11.3	18.6 ± 11.3	CT	Wen et al., 2018
Laurentia									
L990	990	USA	Adirondack fayalite granite	-28.4	132.7	6.9		N+R	Brown and McEnroe, 2012
L970	970	USA	Adirondack anorthosites	-25.1	149.0	11.6		N+R	Brown and McEnroe, 2012
L960	960	USA	Adirondack microcline gneiss	-18.4	151.1	10.5		N+R	Brown and McEnroe, 2012
L950	950	USA	Magnetawan metaseds	-24.0	130.0				McWilliams and Dunlop, 1975
L900	900	USA	Nankoweap Formation	-10.0	163.0	3.5/9.3	-2.1 ± 5.0	N+R	Weil et al., 2003
South China									
SC824	824	Yanbian	Mafic dykes	45.1	130.4	19.0	57.9 ± 20.6		Niu et al., 2016
SC821	821	Hubei	Xiaofeng dykes	13.5	91.0	10.5/11.3	64.5 ± 10.9		Li et al., 2004
SC805	805-802	Hunan	Madiyi Formation	35.3	67.9	4.7/5.5	53.8 ± 4.8	N+R	Xian et al., 2020
SC800	800	Yunnan	Chengjiang Formation	32.8	56.3	7.1/8.6	49.3 ± 7.8	N+R	Jing et al., 2020

Brown, L.L., and McEnroe, S.A., 2012, Paleomagnetism and magnetic mineralogy of Grenville metamorphic and igneous rocks, Adirondack Highlands, USA: Precambrian Research, v. 212–213, p. 57–74, https:// doi .org /10 .1016 /j .precamres .2012 .04 .012.

Jing, X., Yang, Z., Evans, D.A.D., Tong, Y., Xu, Y., and Wang, H., 2020, A pan-latitudinal Rodinia in the Tonian true polar wander frame: Earth and Planetary Science Letters, v. 530, p. 115880, https://doi .org/10.1016/ j.epsl.2019.115880.

Li, Z.X., Evans, D.A.D., and Zhang, S.H., 2004. A 90 spin on Rodinia: possible causal links between the Neoproterozoic supercontinent, superplume, true polar wander and lowlatitude glaciation. Earth Planet. Sci. Lett. 220 (3), 409–421. doi:10.1016/S0012-821X(04)00064-0

McWilliams, M.O., and Dunlop, D.J., 1975, Precambrian paleomagnetism: magnetizations reset by the Grenville orogeny: Science, v. 190, p. 269-272, DOI: 10.1126/science.190.4211.269

Niu, J., Li, Z.-X., and Zhu, W., 2016, Palaeomagnetism and geochronology of mid-Neoproterozoic Yanbian dykes, south China: Implications for a c. 820–800 Ma true polar wander event and the reconstruction of Rodinia, in Li, Z.-X., Evans, D.A.D., and Murphy, J.B., eds., Supercontinent Cycles Through Earth History: Geological Society [London] Special Publication 424, p. 191–211, https://doi .org/10.1144/SP424.11.

Weil, A.B., Geissman, J.W., Heizler, M., Van der Voo, R., 2003, Paleomagnetism of Middle Proterozoic mafic intrusions and Upper Proterozoic (Nankoweap) red beds from the Lower Grand Canyon Supergroup, Arizona: Tectonophysics, v. 375, p. 199– 220, doi:10.1016/S0040-1951(03)00339-1

Wen, B., Evans, D.A.D., Wang, C., Li, Y.X., and Jing, X., 2018, A positive test for the Greater Tarim Block at the heart of Rodinia: Mega-dextral suturing of supercontinent assembly: Geology, v. 46(8), p. 687-690, https://doi.org/10.1130/G40254.1

Xian, H., Zhang, S., Li, H., Yang, T., and Wu, H., 2020, Geochronological and palaeomagnetic investigation of the Madiyi Formation, lower Banxi Group, South China: Implications for Rodinia reconstruction: Precambrian Research, v, 336, 105494, https://doi.org/10.1016/j.precamres.2019.105494